Aggregation of hapten-bearing liposomes mediated by specific antibodies

Kyung-Dall Lee,* Aaron B. Kantor,* Shlomo Nir,‡ and John C. Owicki*

*Department of Biophysics and Medical Physics, University of California, Berkeley, and Cell and Molecular Biology Division, Lawrence Berkeley Laboratory, Berkeley, California 94720 USA; and ‡Seagram Centre for Soil and Water Sciences, Faculty of Agriculture, Hebrew University of Jerusalem, Rehovot, 76100, Israel

ABSTRACT We studied specific membrane–membrane interactions mediated by ligand–receptor binding in a model system, which consisted of (*a*) FG_3P, the fluorescein hapten attached to a phospholipid by a peptidyl spacer as described previously (Petrossian, A., A. B. Kantor, and J. C. Owicki. 1985. *J. Lipid Res.* 26:767–773), (*b*) antifluorescein monoclonal antibodies (MAbs), and (*c*) phospholipid vesicles (liposomes) into which the FG_3P was incorporated. The aggregation of the hapten-bearing liposomes by four MAbs was studied by differential centrifugation. The ability of the MAbs to induce vesicle aggregation varied considerably and correlated inversely with affinity. Aggregation by one of the MAbs was studied in more detail by turbidimetry and freeze-fracture electron microscopy of samples frozen throughout the course of the aggregation. Rapid freezing was achieved with a double propane-jet apparatus. The aggregate morphologies and the time evolution of the aggregate size distribution were obtained from the two-dimensional fracture views with a stereological correction. The aggregation kinetics were simulated by considering dynamical aggregation according to a mass-action model with two parameters, the rate constants for antibody-mediated vesicle aggregation and disaggregation. Both rate constants were orders of magnitude lower than the rate constants for the corresponding interactions of antibodies with haptens either in solution or on vesicles under nonaggregating conditions.

INTRODUCTION

Interactions between biological surfaces that are mediated by surface-bound ligands and receptors are fundamental to many significant events in biological systems, such as cell–cell (Edelman, 1983; Bongrand and Bell, 1984; Springer, 1990) or virus–cell interactions (Ohnishi, 1988; Hoekstra and Kok, 1989; Nir et al., 1990). However, characterization of the kinetic and equilibrium parameters of those interactions in most cellular systems has been difficult due to the complexity of the system.

We reported a model system constructed in our laboratory to investigate several aspects of the ligand–receptor interaction at membrane surfaces (Petrossian and Owicki, 1984; Stanton et al., 1984; Petrossian et al., 1985). The membrane used was a well-defined lipid vesicle into which a hapten, fluorescein, was readily incorporated at a controllable concentration. The fluorescein was anchored to the bilayer through a tripeptide (gly_3) linkage to dipalmitoyl-phosphatidylethanolamine, a construct called FG_3P. The ligands in solution were monoclonal antibodies (MAbs) with known affinity constants specific for the fluorescein moiety of FG_3P. Those studies were confined to intravesicle binding of the antibodies, where an antibody bound to one or two haptens on the same vesicle.

Here we focus on intervesicle binding, where the antibody cross-links haptens on two liposomes, aggregating them. This process mimicks membrane–membrane interactions via specific ligand and receptors as well as the agglutination reaction of antigens by antibodies, which is part of the defense mechanism in the immune system. It also has direct applications to immunoassays based on liposome aggregation (Kung et al., 1985; Mansbach et al., 1985).

We have used complementary methods to study the aggregation process at its late and early stages. As we indicated in a preliminary report, differential centrifugation gives information about the formation of large aggregates late in the process (Kantor et al., 1986). Here we report results for four different antifluorescein MAbs.

We have studied the early stages of aggregation of vesicles by one of the MAbs in detail, using turbidimetry and freeze-fracture electron microscopy (EM) to yield information about kinetics of aggregation and morphology of the aggregates. Turbidimetry has been used previously to study the aggregation of negatively charged vesicles induced by high concentration of Na^+ (Day et al., 1980), as well as that of glycolipid-containing liposomes mediated by specific lectins (Curatolo et al., 1978; Goodwin et al., 1982). Turbidimetry, like most spectroscopic methods, monitors only average parameters related to bulk properties of the aggregation state. Microscopic visualization makes it possible to estimate the distribution of the sizes of aggregates. We have interpreted the EM data using a model of dynamic aggregation previously developed to treat cation-induced vesicle aggregation (Bentz and Nir, 1981; Nir et al., 1983), modified here to account for specific ligand–receptor interactions.

EM also reveals the morphology of the aggregates, as has been shown in previous studies on the cation-induced aggregation of vesicles (Day et al., 1980; Hui et al., 1988). Here we report for the first time morphological

K.-D. Lee's present address is Department of Neurobiology, Harvard Medical School, Boston, MA 02115.

A. B. Kantor's present address is Beckman Center B007, Stanford University Medical Center, Stanford, CA 94560-5125.

J. C. Owicki's present address is Molecular Devices Corporation, 4700 Bohannon Drive, Menlo Park, CA 94025.

Address correspondence to John C. Owicki, Molecular Devices Corporation, 4700 Bohannon Drive, Menlo Park, CA 94025.

TABLE 1 **Characteristics of MAbs**

MAb	Isotype	K^*
		μM^{-1}
2-3-6	IgG_1	500
2-27-12	IgG_1	60
4-4-20	IgG_{2a}	1,000‡
6-19-1	IgG_{2b}	3

* Affinity for sodium fluorescein; affinity of Fab for FG_3P on vesicles is equivalent. Conditions: BBS, pH 8.5, 25°C.
‡ Affinity for hapten on vesicles increases beyond this value for incubations lasting hours (Kantor, 1988).

information on aggregates induced by a specific ligand–receptor interaction.

MATERIALS AND METHODS

Liposomes

The lipid vesicles (liposomes) used were composed of dipalmitoylphosphatidylcholine (DPPC)/cholesterol (2:1). The DPPC (Avanti Polar Lipids, Birmingham, AL) was one spot on thin layer chromatography with developing solvents (chloroform/methanol/water = 65:25:4) and (chloroform/methanol/acetic acid/water = 65:25:4:2) on analytical silica gel 60 plates (E. Merck, Darmstadt, Germany). FG_3P was prepared as reported previously (Petrossian et al., 1985). The lipids were dissolved in chloroform and mixed with FG_3P dissolved in methanol. The mixture was completely dried in a round-bottom flask by rotary evaporation (Haake-Buchler, Saddle Brook, NJ). The lipids were hydrated overnight at 50°C with borate buffered saline (BBS; with 25 mM borate, at pH 8.5, and at osmolarity of 310 mosM adjusted with NaCl, using a freezing-point depression osmometer). The resulting multilamellar vesicles went through five cycles of freezing (liquid nitrogen) and thawing (50°C) and were subsequently extruded through filters of defined pore sizes as described in Szoka et al. (1980) and Mayer et al. (1986). The extrusion was through two stacked polycarbonate filters (Nuclepore, Pleasanton, CA) of final pore size 50 nm, by a high-pressure vesicle extruder (HPVE-10, Sciema Technical Services, Richmond, BC, Canada) at 50°C, yielding essentially unilamellar vesicles with a size distribution of diameters having a mean of 58.1 nm and standard deviation of 11.4 nm, based on a stereological analysis of freeze-fracture data (Lee, 1988). Some nonspecific formation of small aggregates developed over a period of several days. Therefore, experiments were performed on vesicles within 3 d of preparation (≥90% monomers by EM).

Antibodies

Four hybridomas secreting antifluorescein antibodies were obtained from E. W. Voss, Jr. (University of Illinois, Urbana) (Kranz and Voss, 1981; Reinitz and Voss, 1984). The MAbs were purified from Balb/c ascites fluid by protein A affinity chromatography, as described by Kantor (1988). Before experiments, stock antibody solutions were centrifuged at 60,000 *g* for 45 min to eliminate aggregated antibodies.

Table 1 lists the identifying numbers, isotypes, and affinities toward sodium fluorescein for the MAbs. Affinities were determined by the quenching of hapten fluorescence in BBS at 25°C as described by Petrossian and Owicki (1984).

The affinities for FG_3P were obtained with Fab fragments of the four MAbs, which were prepared by papain digestion (Kantor, 1988). Except for MAb 4-4-20, the affinity of each fragment for FG_3P on vesicles was nearly equivalent to the affinity of the native antibody for sodium fluorescein (i.e., to within 20%), as judged by the fluorescence-quenching assay. For binding on the time scale of minutes, the Fab fragments of MAb 4-4-20 also displayed the same affinity for hapten-containing vesicles as for sodium fluorescein. However, on the time scale of hours the affinity increased, becoming at least 10-fold higher by 24 h. The cause of this phenomenon is unknown, but the intact MAb also showed a time-dependent increase in functional affinity (Kantor, 1988).

Differential centrifugation for large precipitants

The vesicles contained 0.25–2.0 mol% FG_3P and were radiolabeled with ^{14}C-DPPC (Amersham, Arlington Heights, IL). Before the addition of antibody, they were centrifuged at 12,000 *g* for 30 min to remove a small number of nonspecific aggregates. Antibodies and vesicles were mixed in microfuge tubes and incubated for up to 24 h. Differential centrifugation monitors the formation of aggregates that are large enough to precipitate under the experimental conditions; smaller ones remain in solution. If an antibody-coated vesicle has a density of 1.05 g/ml, then centrifugation at 12,000 *g* for 5 min over a distance of 5 mm should substantially pellet aggregates with a radius $>2 \times 10^{-5}$ cm. Thus, aggregates of much fewer than 100 vesicles should remain in the supernatant. The radioactivity in an aliquot of the supernatant was used to monitor the centrifugal separation.

Turbidity measurements

The turbidity was measured in a spectrophotometer (Beckman Instruments, Inc., Fullerton, CA) in kinetic mode at wavelength 680 nm, path length 1 cm. The turbidity change is expressed as a percent of initial turbidity. The initial turbidity (O.D.) at time zero is set equal to the optical density of liposomes without antibodies, corrected for the dilution.

Freeze-fracture EM

The time course of the aggregation initiated by addition of antibody was directly visualized by freeze-fracture EM. The aggregation reaction was carried out at room temperature without stirring. Periodically, small aliquots were withdrawn for analysis, and a rapid-freezing method was applied to stop the process of aggregation in milliseconds.

The freezing method has been described in our previous technical reports (Lee and Owicki, 1989*a*, *b*). Briefly, the liposomes were sandwiched between two copper specimen carriers (BU 012 056-T; Balzers, Hudson, NH) with a 400 mesh EM grid attached to each carrier and rapidly frozen by a Gilkey-Staehelin propane jet ultrarapid freezer (model MF7200; Research & Manufacturing Co., Tucson, AZ) (Gilkey and Staehelin, 1986). Such rapid-freezing methods have proved superior to conventional immersion-freezing methods in other morphological and quantitative studies (Heuser and Reese, 1981; Bearer et al., 1983; Kachar et al., 1986; Hui et al., 1988).

The cryo-fixed liposome solution was fractured in a Balzers Freeze-Etch unit BA360M with double replica device (BB 187 269-T; Balzers). The replicas were examined in a Zeiss 109 (Carl Zeiss Inc., Thornwood, NJ) or JEOL 100CX (JEOL U.S.A. Inc., Peabody, MA) electron microscope. Micrographs from two independent runs of experiments were pooled to construct the evolution of aggregate size distribution. For each time point, 400–1,000 vesicles were counted to obtain the apparent distribution of monomers, dimers, and so on.

Analysis of antibody–vesicle binding before aggregation

The following conditions of lipid, hapten, and antibody concentration were used for the EM experiments. For 10 mM DPPC, 5 mM cholesterol, and a mean vesicle diameter of 58 nm, the concentration of liposomes is 0.4 μM. The hapten FG_3P was introduced as 0.05 mol% of lipid or a mean of 12 on the outer lipid monolayer of a vesicle, assuming the same lateral density of FG_3P on the inner and outer mono-

layers. Given a concentration of 850 nM antibody binding sites and assuming bivalency, there were 1.1 antibody molecules per vesicle in the system.

Before calculating the kinetics of vesicle aggregation, we calculated the distribution of vesicles containing 0, 1, 2 · · · antibodies. Antibodies were assumed to bind monovalently to haptens on vesicles; the concentrations of bound and free antibodies and haptens were obtained by solving the following equation:

$$\mathrm{MAb} \cdot H/[(\mathrm{MAb}_0 - \mathrm{MAb} \cdot H)(H_0 - \mathrm{MAb} \cdot H)] = 2K, \quad (1)$$

where MAb_0 and H_0 are the total concentrations of antibodies and (external) haptens, and $\mathrm{MAb} \cdot H$ is the concentration of bound antibodies or haptens. K is the affinity constant, and factor of two accounts for the bivalency of the antibodies.

For $\mathrm{MAb}_0 = 0.43\ \mu\mathrm{M}$, $H_0 = 4.5\ \mu\mathrm{M}$, and $K = 3\ (\mu\mathrm{M})^{-1}$, 96% of the antibodies and 9% of the haptens were bound. The distribution of antibodies on vesicles was obtained from the binomial distribution, assuming that antibodies bound independently and with equal probability to each of 12 haptens on a vesicle. The percentages of vesicles containing 0, 1, 2, 3, and >3 antibodies were, respectively, 32, 38, 21, 7, and 2.

Some of the antibody may bind bivalently to a single vesicle and hence possibly be unavailable to participate in the aggregation process, at least at short times. Thus, computations were also done assuming 30% intravesicular bivalent binding.

Construction of the stereologically corrected distribution of aggregate sizes from the apparent distribution

The apparent aggregate size distribution was obtained by counting the liposomes in the freeze-fracture replicas. When the fracture passes through an aggregate, it may not reveal all the vesicles in the aggregate; the apparent size distribution tends to be skewed toward smaller aggregates. A precise correction for this process would take into account the morphologies of the aggregates and the factors that influence the path of the fracture (e.g., whether it passes straight through aggregates or follows the contours of the vesicles within a cluster). An opposite bias in the apparent distribution (toward large aggregates) would occur if the fracture preferentially occurred at large aggregates, which are regions of low resistance to fracture. In the absence of clear information about these effects, we have presented the apparent distribution and a corrected distribution based on an approximate stereological treatment.

Let $P(m, n)$ be the probability that an actual n-mer, once sectioned by the fracture plane, appears as an m-mer ($m \leq n$) in the freeze-fracture replica. Monomers always fracture as monomers; $P(1, 1) = 1$. The probability that a dimer appears as a monomer, $P(1, 2)$, is equal to $1 - P(2, 2)$. The value of $P(2, 2)$ is rigorously one half for spheres of equal size in contact and an unbiased fracture plane, as is illustrated in Fig. 1.

The calculation for trimers is more complex, since morphology plays a great role in determining the probability. Not fully accounting for three-body correlations among vesicle positions, we approximate $P(1, 3)$ by $P(1, 2) \times P(1, 2) = 1/4$, and so $P(2, 3) + P(3, 3) = 1 - P(1, 3) = 3/4$. The conditional probability of the third vesicle being cut by the fracture plane when the other two are already cut is about the same as $P(2, 2)$. Therefore, $P(3, 3) \approx P(2, 2) \times [P(2, 3) + P(3, 3)]$. This suggests the following recursion relationship that approximates $P(m, n)$ for larger aggregates:

$$\text{for } m = 1, \quad P(1, n) = (1/2)^{n-1},$$

and

for $m > 1$,

$$P(m, n) = [1 - P(1, n)] \times P(m - 1, n - 1). \quad (2)$$

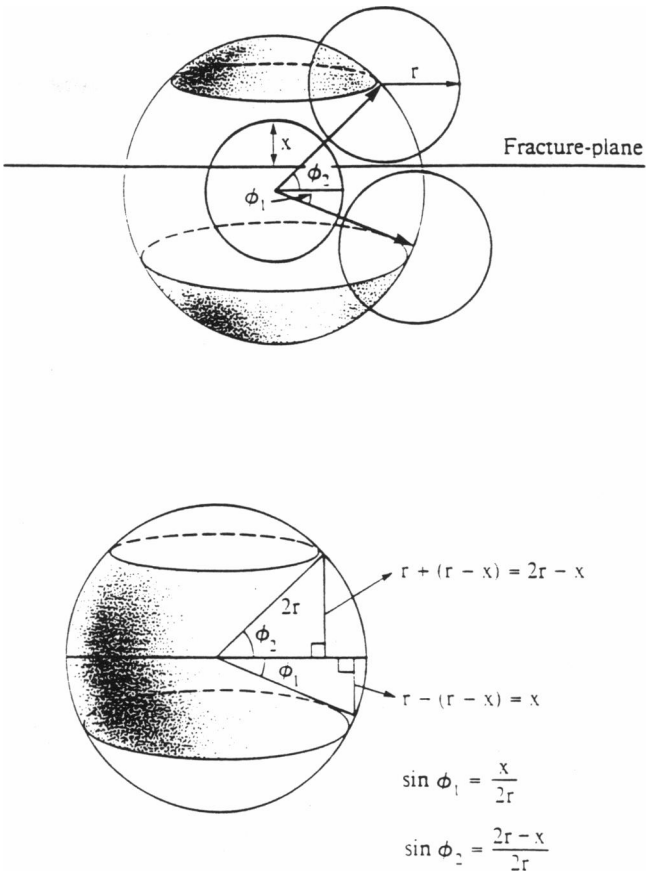

FIGURE 1 Calculation of $P(1, 2)$. $P(1, 2)$, the probability that a fractured dimer appears as a monomer, is represented in the upper cartoon by the shaded area on the surface of a sphere with a radius $2r$; r is the radius of the vesicle and $r - x$ is the distance between the fracture plane and the center of the first vesicle fractured. The center of the second vesicle can be randomly positioned on the surface of the sphere with radius $2r$. Then $P(2, 2)$, the probability that the fracture passes through the second vesicle, is equal to the probability that angle ϕ lies in the range $(-\phi_1, +\phi_2)$, where $\sin(\phi_1) = x/2r$, $\sin(\phi_2) = (2r - x)/2r$. Thus, $P(1, 2) = 1 - P(2, 2) = 1/2$.

The stereological correction is performed by solving a system of linear equations. A corrected distribution $(c_1, c_2, \ldots, c_n)$ is calculated from the apparent aggregate size distribution $(a_1, a_2, \ldots, a_n)$ according to the matrix equation $a_i = \sum P_{ij} \times c_j$, where a_i and c_i represent the molar concentrations of i-mer and $P_{ij} = P(i, j)$.

Theoretical procedure for calculating kinetics of antibody-induced aggregation of vesicles

A comprehensive theoretical model of the aggregation would take into account factors such as the polydispersity of both antibodies and haptens on vesicles, perturbations of antibody–vesicle binding by the aggregation process, and the morphology of the aggregates. Such a model would be difficult to construct, and its validation would require more extensive data than we have collected. Instead, we have used a simplified theoretical treatment, based on one described by Nir et al. (1983, 1986*a*), to obtain order-of-magnitude information about the aggregation and disaggregation kinetics of vesicles. Attempting to minimize the number of adjustable parameters without sacrificing the essential features of the process, we have used two: $C\ (\mathrm{M}^{-1}\ \mathrm{s}^{-1})$, the rate con-

stant of vesicle aggregation, and D (s^{-1}), the rate constant of vesicle disaggregation. We also have ignored most of the dependence of aggregation rate on the size and morphology of the interacting aggregates.

Following are the rules that govern the model aggregation process. The notation $A(I, J)$ denotes the molar concentration of aggregate of $(I + J)$ vesicles, formed from I vesicles with one or more antibodies available for binding to other vesicles and J vesicles that do not contain antibodies.

(a) The antibody–vesicle binding equilibrium is assumed to be established before the beginning of aggregation, and these antibodies are then deemed permanently attached.

(b) Vesicles are divided into two homogeneous categories: those with and those without bound antibodies. Antibody-containing vesicles are treated as monovalent with respect to available antibody binding sites. The multiple haptens on a vesicle are not treated individually. A consequence is that an aggregate can contain no more than one antibody-free vesicle. In other words, J is either 0 or 1, but I is unconstrained. For example,

$$A(1, 0) + A(0, 1) \rightleftharpoons A(1, 1) \quad , \tag{3}$$

but no further aggregation can occur for

$$A(1, 1) + A(0, 1) \quad . \tag{4}$$

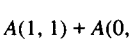

(c) When two vesicles bind, each containing an available antibody binding site, only one of the vesicle's antibodies forms the bond between vesicles (i.e., no double-bonded vesicles):

$$A(1, 0) + A(1, 0) \rightleftharpoons A(2, 0) \quad . \tag{5}$$

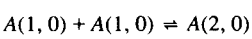

(d) The association rate constant for $A(I_1, J_1)$ and $A(I_2, J_2)$ to form $A(I_1 + I_2, J_1 + J_2)$ is proportional to the number of antibody-vesicle interactions: $(\delta_{J1,0} + \delta_{J2,0}) \times C$, where $\delta_{i,j}$ is equal to 1 if i = j and 0 otherwise. In other words, the rate constant is 0, C, or $2C$, depending on whether neither, one, or both the aggregates has a free antibody.

(e) After some experimentation with rules for disaggregation, disaggregation was allowed for $A(I, 1)$ and $A(2, 0)$ aggregates but not for $A(I, 0)$, $I > 2$. The following depiction can help explain the rationale:

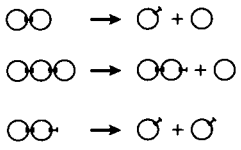

In the case of trimers and larger aggregates of the type $A(I, 0)$, cyclization is possible, and this multivalent interaction should lend increased stability:

Hence the aggregates $A(I, 0)$, $I > 2$ were assumed to be formed irreversibly.

(f) Where disaggregation was allowed, the rate constant for dissociation of each bond was D. The computation was based only on the disaggregation of linear aggregates. Although bivalent antibody-mediated bonds between vesicles are symmetric, disaggregation was assumed to take place only at the binding site where aggregation occurred. In other words, antibodies remained permanently attached to the vesicles to which they were bound before the aggregation.

The computer program solves the nonlinear differential equations of aggregation kinetics by means of a Taylor expansion. It allows for any maximum aggregate order, M, but in practice $M = 13$ was sufficient; the results for $M = 9$ or 21 gave similar answers. C and D are adjusted to minimize the sum of the squares of differences between theoretical and experimental aggregate distributions.

RESULTS AND DISCUSSION

Differential centrifugation experiments

The four anti-fluorescein MAbs differed significantly in their ability to precipitate the liposomes (2.9 nM vesicles, hapten 1 mol% of lipid). As shown in Fig. 2 A, all except MAb 4-4-20 displayed well-defined maxima in the curves for amount of precipitation vs. antibody concentration. Two of the MAbs, 2-27-12 and 6-19-1, precipitated almost all the vesicles at this maximum (near 300–400 nM); MAb 2-3-6 precipitated only 40% (near 90 nM), and MAb 4-4-20 at most 10% (throughout a broad concentration range). Precipitation was specific to the antibody-hapten interaction: vesicles without hapten were not precipitated by MAb and nonspecific rabbit IgG did not precipitate the hapten-bearing vesicles.

The time course of the precipitation is shown in Fig. 2 B, where the concentration of each MAb was chosen to be near that giving maximum precipitation in Fig. 2 A. The process proceeds in two steps. First, within a few seconds, the MAb binding to the vesicles comes to equilibrium, as judged by the completion of fluorescence quenching (data not shown). Second, on a time scale of hours, antibody bridges form between the vesicles and lead to aggregation. Using a similar dansyl hapten/liposome/MAb model system, Luedtke and Karush (1982) observed precipitation kinetics consistent with the data presented here for MAbs 6-19-1 and 2-27-12.

The MAb concentration at which maxima, such as those shown in Fig. 2 A for 6-19-1 and 2-27-12, occur ($MAb_{0,max}$) is linearly proportional to vesicle concentration at constant mole percent hapten. Similarly, decreasing the mole percent hapten (when <1%) leads to a reduction in the amount of antibody required for maximum precipitation and a decrease in the rate of aggregation (Kantor, 1988).

The existence and nature of these maxima follow from theoretical considerations (von Schulthess, 1976), concluding that aggregation should be maximized when half the hapten sites are free and half are monovalently bound by antibody, i.e., when

$$\mathrm{MAb} \cdot H = H = \tfrac{1}{2} H_0. \tag{6}$$

The theoretical and experimental results are consistent with the classical precipitin behavior of antibodies and multivalent antigens (Heidelberger and Kendall, 1935; DeLisi, 1974). At low antibody concentrations, precipitation is limited by the supply of antibodies to cross-link antigens. At high concentrations, antibodies saturate the available binding sites on antigens so that a paucity of free binding sites limits cross-linking. The optimum amount of precipitation occurs when the product of the

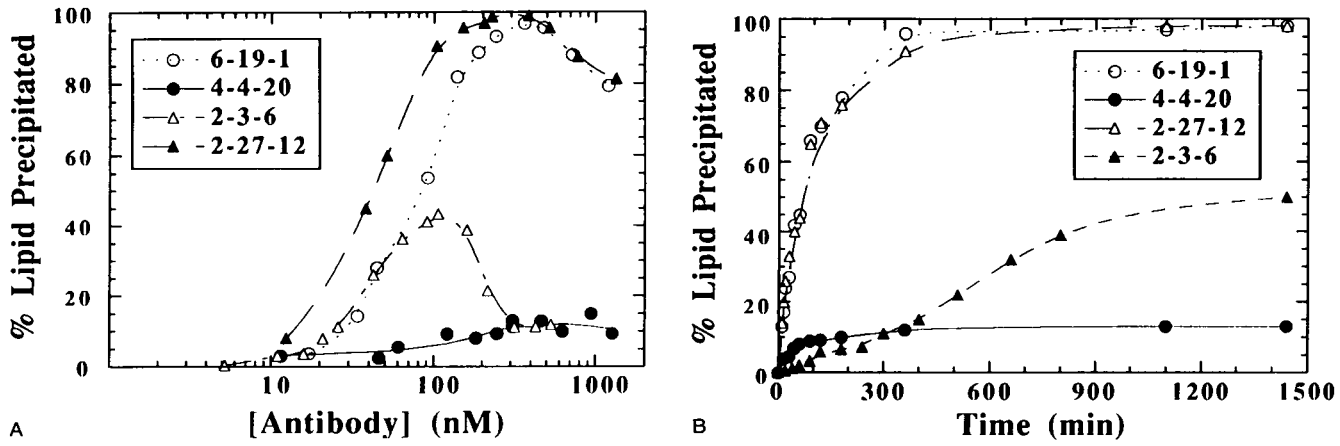

FIGURE 2 Differential centrifugation of large vesicle aggregates. (*A*) Precipitation curves. MAbs were incubated with vesicles (1.0 mol% FG_3P, 200 μM lipid) for 24 h before centrifugation. Vesicles without FG_3P were not precipitated by any MAb. Nonspecific rabbit IgG also does not precipitate the vesicles containing hapten. (*B*) Kinetics of precipitation. Conditions were chosen from data such as Fig. 2 *A* to be near maximum precipitation at long times. Concentrations of MAb and vesicles and mol percent FG_3P were: 2-3-6 (105 nM; 2.9 nM, 1.0%); 2-27-12 (250 nM, 2.9 nM, 1.0%); 4-4-20 (300 nM, 2.9 nM, 1.0%); 6-19-1 (225 nM, 1.43 nM, 0.5%).

concentrations of free hapten sites H and complementary free binding sites of antibodies bound monovalently to antigen MAb · H is maximum. It follows from the von Schulthess model that $MAb_{0,max} \propto H_0$, i.e., $\propto$ the product of hapten mole percent and vesicle concentration. This is indeed observed for MAbs 6-19-1 and 2-27-12.

What factors cause the differences in precipitation behavior of the four MAbs? Conformational effects can be important, as is known for the poor precipitating efficiency of equine IgG(T) (Klinman and Karush, 1967) and differences in efficiency between $(Fab')_2$ and intact IgG (Moller, 1979). Isotype-dependent segmental flexibility has been linked to differences in effector function for murine MAbs (Oi et al., 1984). In our data, the IgG_2's, which are highly flexible, exhibit the extremes of precipitation efficiency. The two IgG_1's, which are less flexible, also include both a good and a modest precipitator. Thus, flexibility does not appear to be a dominating factor here. On the other hand, Fig. 3 shows that the maximum amount of precipitate in Fig. 2 *A* correlates negatively with antibody affinity. Consistent with our results, the anti-dansyl MAb used by Luedtke and Karush (1982) had $K = 100\ (\mu M)^{-1}$ and was a good precipitator of dansyl-bearing liposomes.

It may be that affinity modulates the ability of antibodies to precipitate large aggregates of vesicles by controlling the ratio of (intravesicle) bivalently bound to monovalently bound antibody. On an isolated vesicle, an equilibrium should be established quickly between bivalently bound antibodies and monovalently bound antibodies plus free hapten. Formal mass-action considerations dictate that the ratio of bivalently to monovalently bound antibodies will be proportional to the affinity, K, of antibody for hapten, and another factor, α, that accounts for entropic and steric effects (see, e.g., Crothers and Metzger, 1972). In the equation below, { } indicates lateral (two-dimensional) concentrations of reactants:

$$\{MAb \cdot H_2\} / \{MAb \cdot H\} = \alpha K \{H\}. \qquad (7)$$

All else being equal, strongly binding antibodies such as 4-4-20 initially produce vesicles that are less "sticky" (i.e., have fewer complementary free antibody binding sites and free hapten) than do more weakly binding antibodies such as 6-19-1. If reorganization of the antibody binding is required for the extensive aggregation measured in the centrifugation assay (i.e., intravesicle biva-

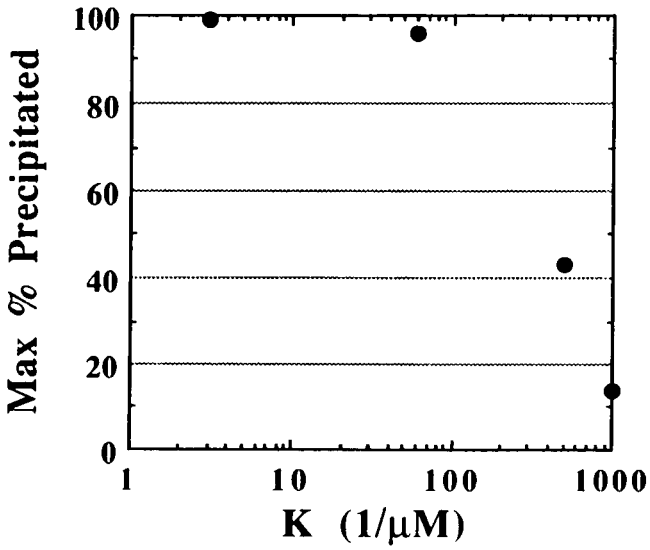

FIGURE 3 Correlation between maximum percent of vesicles precipitated (Fig. 2 *A*) and antibody affinity (Table 1).

lent → monovalent → inter-vesicle bivalent), then high affinity should also limit the aggregation process, because it correlates with slow dissociation kinetics.

Note that this argument requires the aggregation process to be to some extent under kinetic rather than equilibrium control: at equilibrium, affinity per se is neutral with respect to intra- versus intervesicular bivalent binding. The importance of kinetics in multivalent antibody-membrane interactions has been stressed by Mason and Williams (1980).

To test the relationship between aggregation efficiency and affinity more strictly, it clearly would be advantageous to have a wider variety of antibodies. A particularly useful strategy would be to control for conformational factors by testing a series of antibodies with differing affinity produced, e.g., by site-directed mutagenesis in the binding site.

We also studied the ability of an excess of soluble hapten to interfere with the formation of precipitates for the case of MAb 6-19-1. Earlier stages of aggregation (1 mol% FG_3P, 167 μM lipid, 250 nM antibody) can be reversed by the addition of >100-fold excess (200 μM) soluble fluorescein. At 5 and 30 min after antibody addition, the amount of aggregated lipid that can be centrifuged is reduced from 50 and 80% to <3%. However, by 2 h the reaction can be only partially reversed (88 down to 30%). At 24 h, the aggregates cannot be disrupted with either soluble fluorescein or >1,000-fold excess (2 mM) fluoresceinamine (a nonfluorescent analogue of fluorescein that binds the MAb).

Interestingly, however, if the reaction is allowed to proceed in the presence of inhibitor (either level of soluble fluorescein), it still reaches maximum precipitation (95%) by 24 h. We speculate that soluble hapten is able to dissociate small aggregates but not highly interconnected larger aggregates. This may lead to a nucleation-like phenomenon in which the competition between soluble and vesicle-bound hapten for the antibodies leads to dynamic fluctuations in aggregate size: most small aggregates dissociate but aggregates that reach a critical size persist and grow.

Analysis of the early stages of aggregation

We analyzed the early stages of aggregation by MAb 6-19-1, one of the two most effective precipitators in the differential-centrifugation experiments. The most important data were obtained by time-resolved freeze-fracture electron microscopy. This method is restricted to conditions of high vesicle concentration, so that enough aggregates can be visualized conveniently to obtain good statistics. High vesicle concentration implies fast aggregation kinetics, hence it was necessary to reduce the number of haptens per vesicle considerably to slow the process enough that aliquots could be collected and frozen over a period of minutes before the aggregation had proceeded too far. We found turbidimetry a convenient source of semi-quantitative information about the early events in aggregation, and useful for further establishing conditions suitable for electron microscopy as well.

Turbidity experiments

Given that the diameters of the vesicles are near the wavelength of visible light, interference effects make it hard to interpret turbidity changes quantitatively in terms of degree of aggregation. The antibody by itself in solution did not contribute significantly to the turbidity. Nevertheless, the initial binding of the antibodies to the hapten-bearing vesicles resulted in an increase in the turbidity (see curve *D2* in Fig. 4 *A* for the initial increase in the turbidity caused by Fab binding to the vesicles). A similar phenomenon has been reported in other cases (Nelsestuen and Lim, 1977). However, in our case a significant percentage of the turbidity increase within 30 s also can be attributed to vesicle aggregation.

Three control experiments showed that the aggregation was induced by specific intervesicular cross-linking of the hapten-containing vesicles by bivalent antibodies. First, vesicles without the hapten did not aggregate in the presence of MAb 6-19-1 (curve *D1*, Fig. 4 *A*); the changes in the turbidity over 30 min were <2.5% of the level of liposomes alone, indicating that the nonspecific interactions among the vesicles are negligible on the time scale of minutes even in the presence of antibody. Second, using just the monovalent Fab fragments of MAb 4-4-20 did not result in the aggregation of hapten-containing vesicles (curve *D2*, Fig. 4 *A*). Third, the aggregation could be inhibited by a 20-fold excess of soluble fluorescein over FG_3P (curve *D3*, Fig. 4 *A*), which effectively competes with the membrane-bound hapten on the time scale of these measurements. All of the above controls are consistent with the controls for the differential-centrifugation experiments.

MAb 6-19-1 (curve *B*, Fig. 4 *A*) was more effective than MAb 4-4-20 (curve *C*, Fig. 4 *A*) at forming small vesicle aggregates. This is similar to the results of the differential-centrifugation experiments. Doubling the surface concentration of FG_3P from 0.05% (curve *B*) to 0.10% (curve *A*) enhanced the rate of turbidity increase. The decrease in the turbidity at the later stage of aggregation in curve *A* was due to the formation and fast sedimentation of large aggregates out of the light beam in the cuvette. For the conditions monitored, increasing the antibody concentration (Fig. 4 *B*) had a greater effect on the rate of the aggregation than did increasing lateral hapten concentration.

EM: specificity of aggregation and test for fusion

The control experiments done for the turbidimetric measurement and differential centrifugation were also confirmed by freeze-fracture EM; aggregation of vesicles was not induced either by adding Fab fragments to the hap-

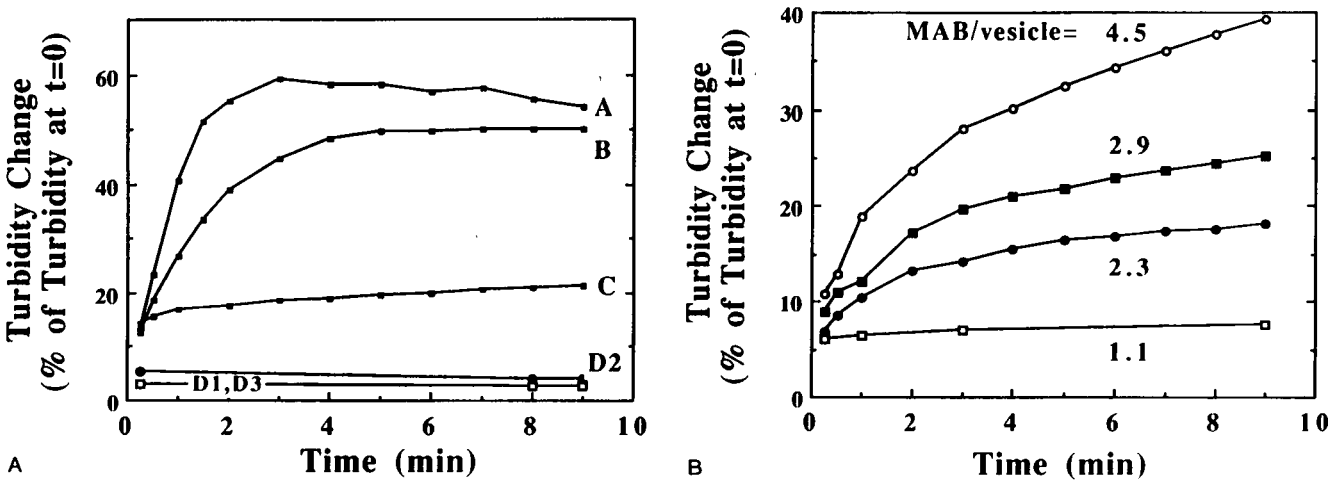

FIGURE 4 (*A*) Aggregation of liposomes monitored by turbidimetry. Curves *A* and *B* show the percent turbidity change upon adding MAb 6-19-1 to vesicles containing 0.10 and 0.05 mol% FG_3P, respectively. Curve *C* shows the aggregation induced by MAb 4-4-20 under the same conditions. Curve *D1* shows the turbidity change upon adding MAb 6-19-1 to the vesicles containing no haptens, curve *D2* upon adding 4-4-20 Fab to the vesicles with hapten, and curve *D3* under the same condition as in *B* except the presence of excess sodium fluorescein. The curves *D1* and *D3* coincided with each other at this scale. For all cases, the lipid concentration was 7.5 mM, and there were 4.5 antibodies per vesicle (1.7 μM binding site concentration). (*B*) Effect of concentration of MAb 6-19-1 on the aggregation rate. Vesicles were incubated with a fourfold range of antibody concentration (1.1–4.5 antibodies added per vesicle). All the vesicles contained 0.05 mol% FG_3P, and the lipid concentration was 3.75 mM.

ten-containing vesicles, by adding antibodies in the presence of excess soluble fluorescein, or by adding antibodies to the vesicles containing no hapten. The possibility of fusion among the aggregated liposomes was eliminated by comparing the size of the vesicles before and after the addition of antibody within the timescale of experiments. The mean and standard deviation of vesicle diameters were 58.1 nm and 11.4 nm before adding antibodies, and 59.6 nm and 11.9 nm afterward; these are not significantly different. Nor were structures observed that resembled fusion intermediates or products (Bearer et al., 1983).

EM: morphology of aggregates

The addition of MAb 6-19-1 to the suspension of monomeric vesicles induced the formation of dimers, trimers, and so on. The typical morphology of these small aggregates is shown in Figs. 5 and 6. Dimers appeared in freeze-fracture replicas either as two adjacent convex (or concave) hemispheres or one convex and the other concave hemisphere. Both cases are shown in Fig. 5. In the latter case, the apparent distance between the vesicles probably approximates the distance of closest approach. This is near the dimensions of an IgG molecule (~10–15 nm). There sometimes appeared a feature in the contact area between vesicles that could have been an IgG molecule bridging the vesicles; this is seen in Fig. 5.

Trimers tended to be triangular rather than linear, as is shown in Fig. 6, but the connections among three vesicles in a trimer were not normally symmetrical. Large aggregates showed a striking difference from the morphology of negatively charged vesicles whose aggregation was induced by cations (Day et al., 1980; Hui et al., 1988). The contact area between the aggregated vesicles was smaller than the contact area in the cation induced aggregation, even in the large aggregates.

EM: evolution of aggregation

The time course of aggregation was followed by EM under conditions where vesicles were concentrated (15 mM lipid, 0.4 μM vesicles) but in which the rate of aggregation was slowed by low antibody and hapten concentrations (1.1 antibodies per vesicle, 0.05 mol% hapten). These conditions are identical to those for the slowest aggregation shown in Fig. 4 *B* except for the fourfold higher concentration of vesicles used for EM.

Fig. 7 (*A* through *D*) shows typical areas of the freeze-fracture replicas at 0, 2, 6, and 15 min after the antibodies were added. The apparent distribution of the aggregate sizes at each time point is shown in Fig. 8 and Table 2. Because the visualized aggregates may represent only sections through larger aggregates, the stereological correction described in Materials and Methods was applied to the apparent distribution; the results are shown in Table 2.

Without knowing more about the processes that direct the fractures, it is difficult to say which data set represents the aggregate distribution more accurately. Fortunately, both show the same qualitative picture of the aggregation process. There is a rapid drop in the percentage of monomeric vesicles during the first 2 min, followed by a much slower decline. Over the period 2–15 min, the percentage of vesicles in dimers tends to fall and that in trimers to rise. The percentage of vesicles in tetramers

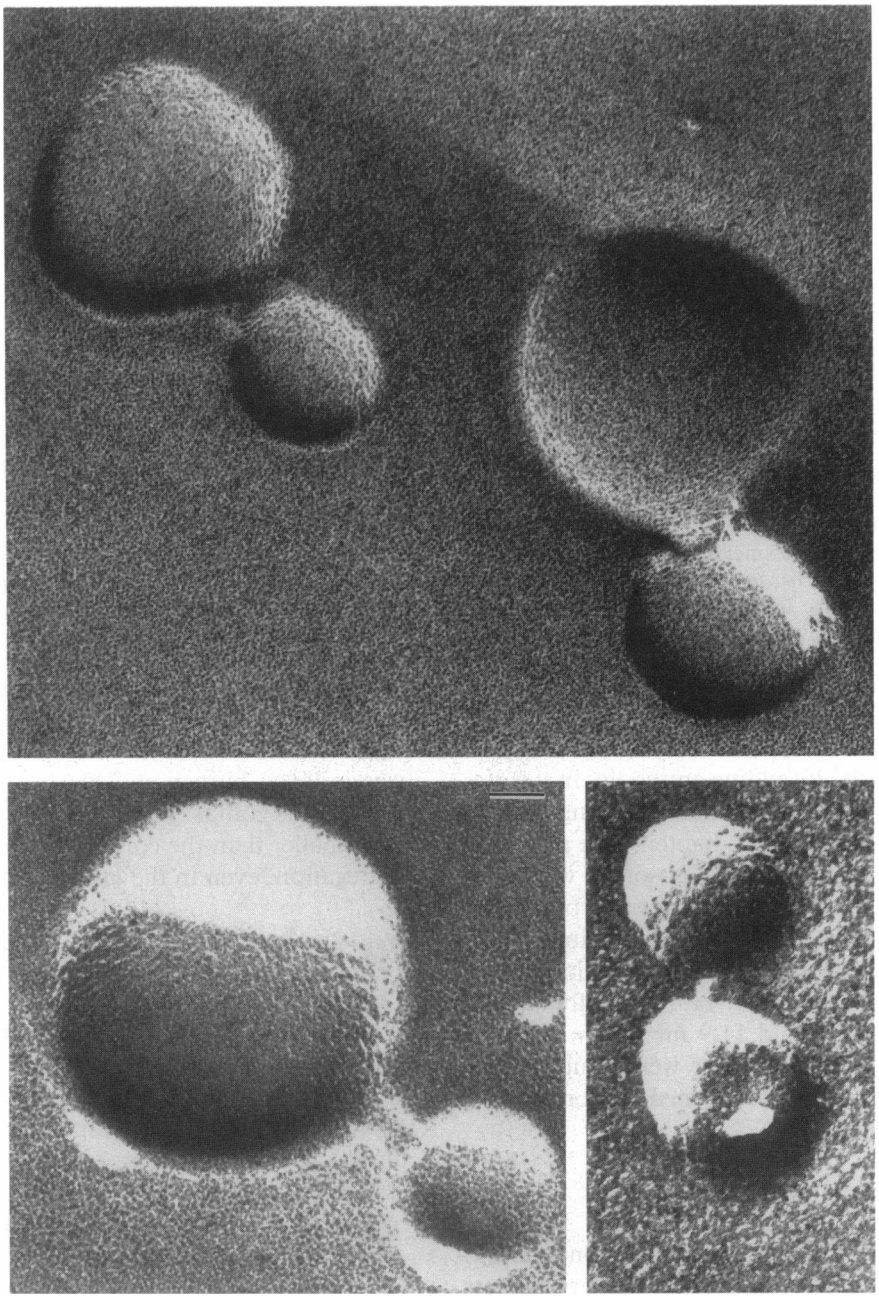

FIGURE 5 Typical freeze-fracture electron micrographs showing the morphology of dimers. The bar represents 0.02 μM.

(or larger aggregates) rises monotonically. The behavior of dimer and trimer percentages, particularly in the corrected distribution, is similar to the rise and fall of intermediates in a sequential chemical reaction.

Perhaps the most striking feature of the data is the failure of the aggregation to go to completion, as judged by monomer content, after a rapid beginning. This largely reflects the stochastic distribution of antibodies among vesicles that leaves about one third of the vesicles without antibodies and therefore unable to participate fully in the aggregation. Likewise, many vesicles do not precipitate at low MAb/vesicle ratios in the differential centrifugation experiments even after 24 h.

Theoretical modeling of aggregation

The aggregation model described in Materials and Methods was fit to the EM results in Fig. 8 by adjusting the forward and reverse rate constants for vesicle aggregation (C and D). Four different fits were performed (Table 2): to the apparent and stereologically corrected data and assuming that either none or 30% of the antibodies

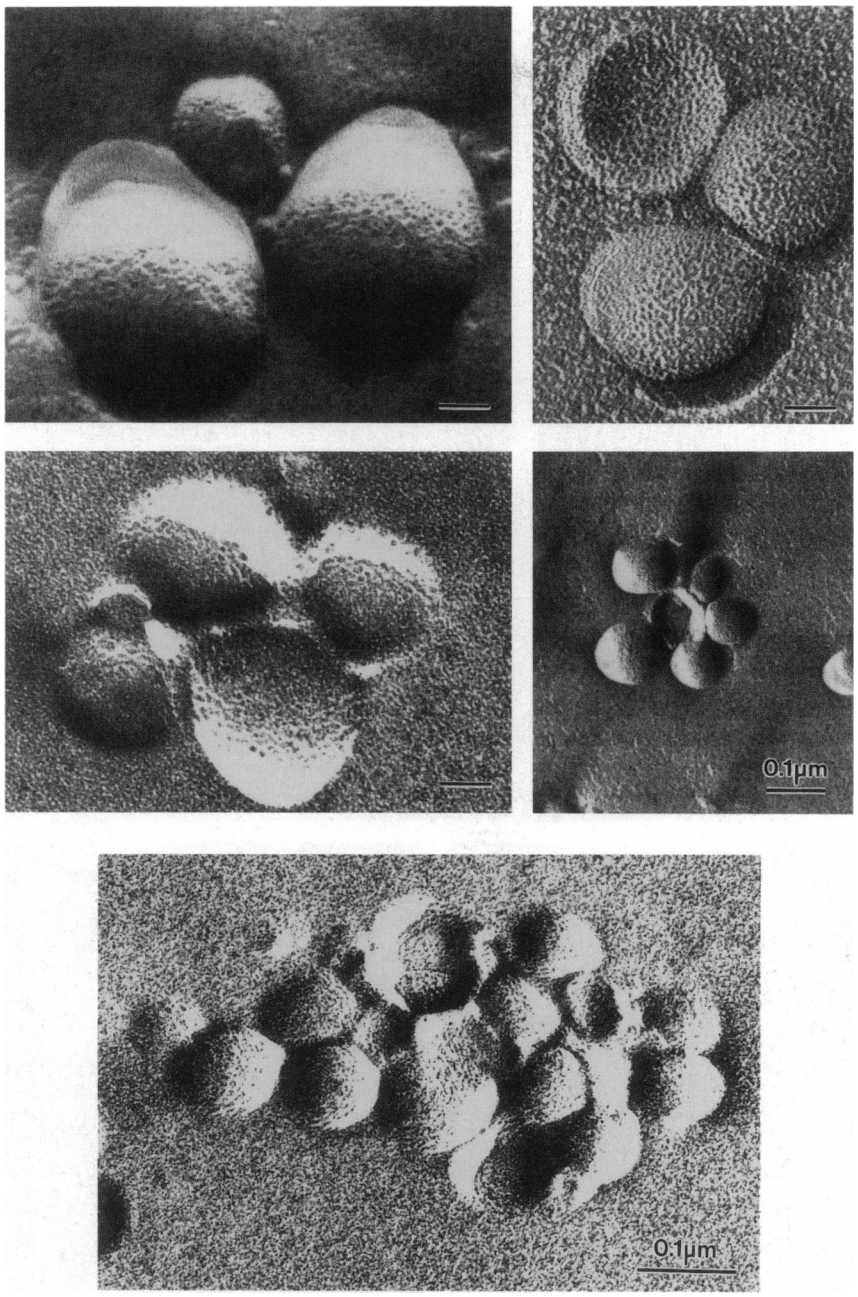

FIGURE 6 Typical freeze-fracture electron micrographs showing the morphology of trimers and larger aggregates. These micrographs were taken during the experiments reported in Figs. 7 and 8. The bars represent 0.02 μm except where noted otherwise.

bound bivalently intravesicularly and thereby were removed from the aggregation process.

The sensitivity of the fit to values of the adjustable parameters C and D is similar for all four calculations shown in Table 2. When D is varied by 10% about its optimum (with C fixed), the root-mean-square (RMS) error of the fit rises by 2% (i.e., is multiplied by 1.02). Similarly, varying C and fixing D yields a 10% rise. Thus, the goodness of fit is less sensitive to small variations in D than in C. When C and D are simultaneously doubled (keeping their ratio, a measure of affinity, fixed), the error increases by 50%; when they are halved, the error increases threefold. The decision to allow dimers of type $A(2, 0)$ to disaggregate was motivated by an overestimate of dimer concentrations when such disaggregation was not allowed.

The amount of intravesicle bivalency affected the character of the fit in a minor way but the values of C and D almost not at all. The fit to the apparent data was significantly better than to the corrected data; the values of C differed by about threefold and those of D were nearly the same. Considering these factors as well as the sensitiv-

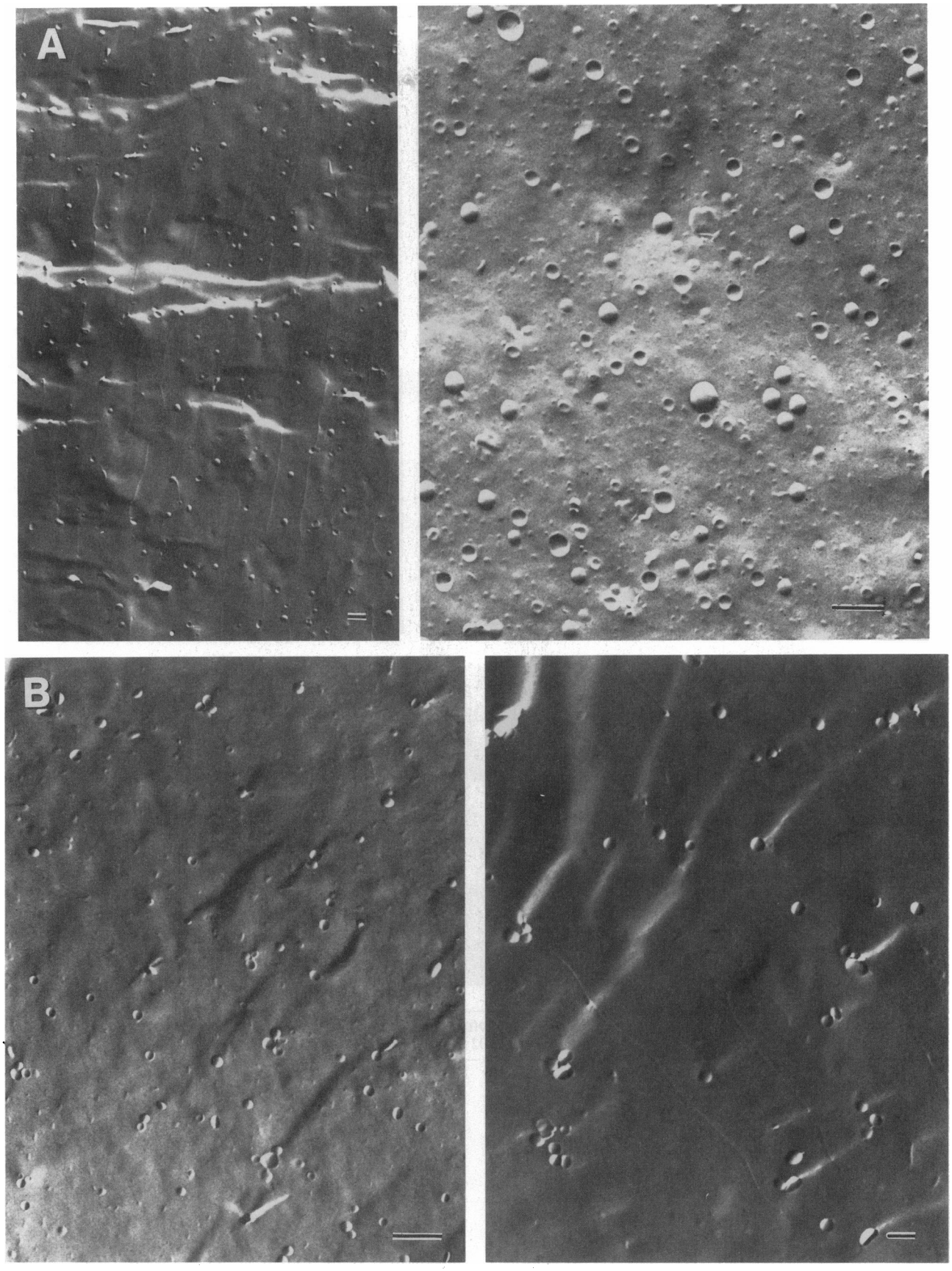

FIGURE 7 Typical freeze-fracture electron micrographs showing the evolution of vesicle aggregation. The aggregation was monitored at 0 min (*A*), 2 min (*B*), 6 min (*C*), and 15 min (*D*) after adding antibodies. Lipid concentration was 15 mM, antibody binding site concentration 850 nM, FG_3P concentration 0.05 mol% of lipids. The bars represent 0.2 μm.

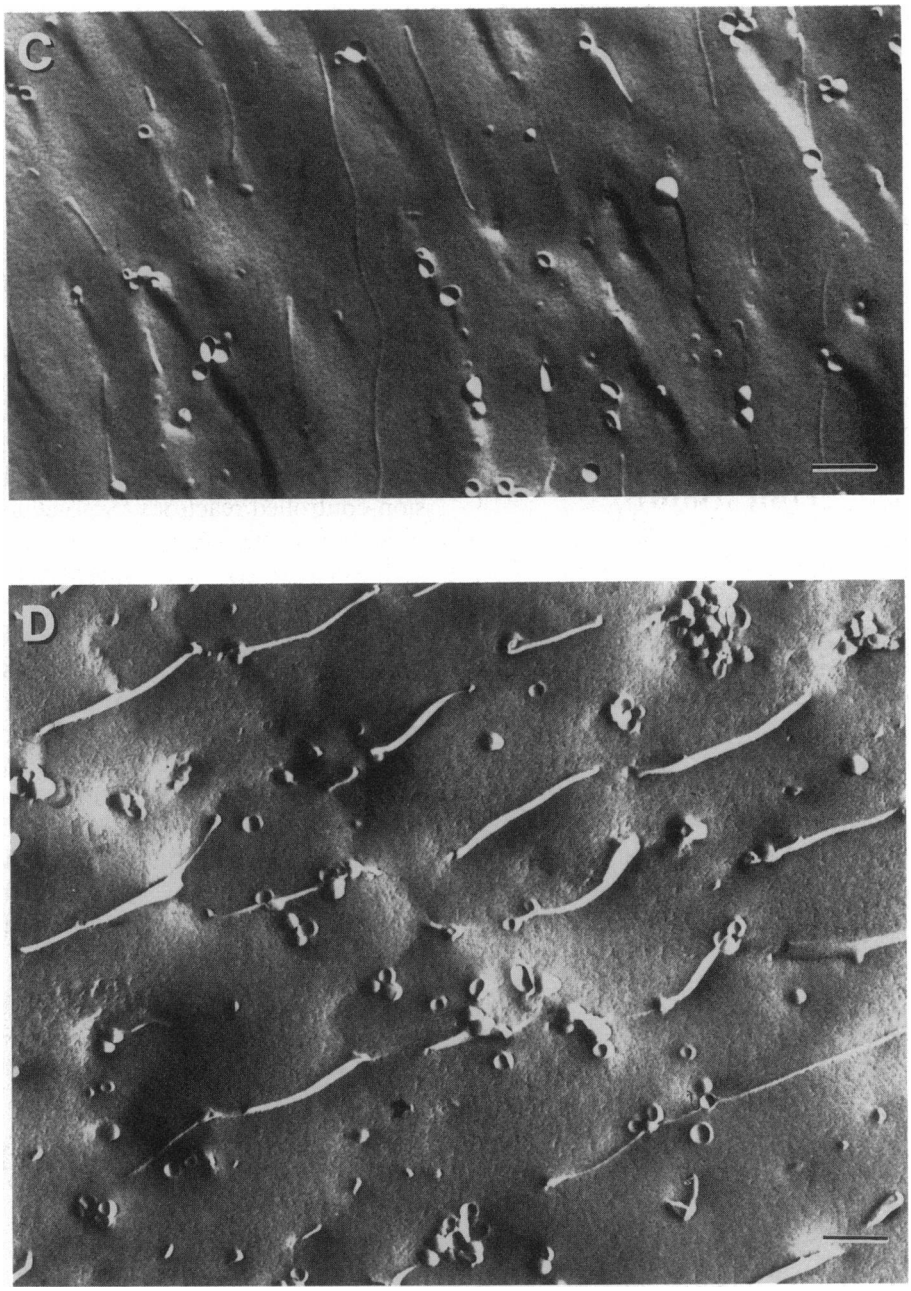

FIGURE 7 (continued)

ity of the RMS error discussed above, we estimate that the most realistic value of C lies in the range 2×10^4 to $1 \times 10^5\ M^{-1}\ s^{-1}$, whereas that for D is roughly 4×10^{-3} to $1 \times 10^{-2}\ s^{-1}$.

These rate constants for aggregation and disaggregation are one to two orders of magnitude lower than the corresponding values for the interaction of Fab fragments with the same hapten-bearing vesicles ($1.6 \times 10^6\ M^{-1}\ s^{-1}$ and $0.5\ s^{-1}$, determined by fluorescence-quenching methods similar to those of Petrossian and Owicki, 1984). Given that C is expressed in terms of concentration of vesicles, each of which contains 12 haptens, the effective reduction in the rate constant for formation of antibody-hapten bonds is really two to three orders of magnitude. The rate constants for Fab interacting with FG_3P on a vesicle are themselves three to four times lower than the rate constants for Fab or antibody interacting with sodium fluorescein ($5 \times 10^6\ M^{-1}\ s^{-1}$ and $2\ s^{-1}$).

Thus, there is a strong trend toward lower rate constants as the antibody and hapten are attached to bulky carriers. The larger diffusive size of the vesicle-bound reactants, coupled with a restricted reactive area and the potential barrier for a close approach of vesicles, presumably contribute to this trend (see, e.g., DeLisi, 1980). Conformational constraints that make it difficult for an

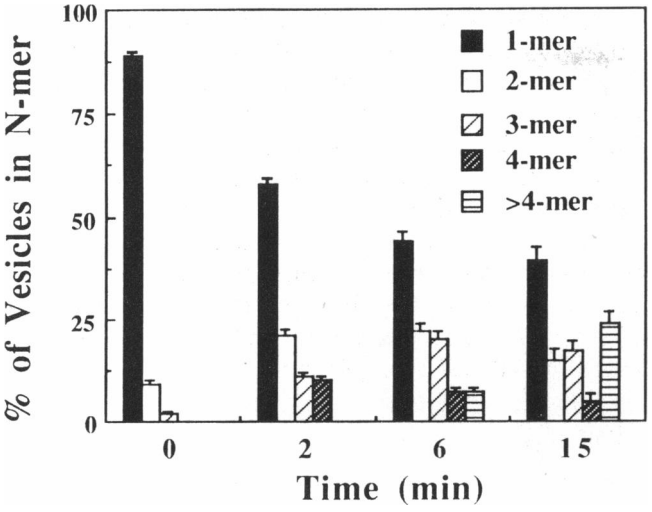

FIGURE 8 Apparent aggregate-size distribution obtained from freeze-fracture EM. Data are presented as percent of vesicles in each aggregate size and were pooled from two independent experiments to construct the distribution of aggregate size at 0, 2, 6, and 15 min after the addition of antibody. The conditions were the same as in Fig. 7. A total of 1,000 vesicles each was counted for the 0- and 2-min time points, and 400 each for the 6- and 15-min time points.

antibody simultaneously to bind haptens on apposed vesicles also may be present. The decrease in association/aggregation rate is orders of magnitude too large to be explained solely by antibody-hapten binding operating with translational diffusion coefficients appropriate for vesicles. The slowing of kinetics due to the inhomogeneous three-dimensional distribution of membrane-bound reactants analyzed by Berg and Purcell (1977) is not important here, both because the reactions in our system are not appreciably under diffusion control and because the distribution is not sufficiently inhomogeneous. Additional data, perhaps obtained with different MAbs, would be required to narrow the possibilities for the mechanism of the slowing.

Our results also can be compared with aggregation processes that are not mediated by ligand–receptor-like interactions, i.e., when similar size particles are uniformly reactive over their entire surface. The value of C found in our studies is four orders below that in diffusion-controlled reactions (Smoluchowski, 1917) or two orders of magnitude below that in (650 mM) Na^+-induced or (2 mM) Ca^{2+}-induced aggregation of phosphatidylserine vesicles (Day et al., 1980; Bentz and Nir, 1981; Nir et al., 1983; Hui et al., 1988).

The ratio C/D for our system, which can be interpreted as an affinity for dimer formation, is probably in the range 2×10^6 to 2×10^7 M^{-1}. To be compared with the affinity of Fab for hapten on the vesicle (3×10^6 M^{-1}), this should be divided by the number of haptens per vesicle (12), giving a range of 2×10^5 to 2×10^6 M^{-1}. It is reasonable that steric effects involved in cross-linking vesicles should lower the affinity, but one must be wary of overinterpreting the results of this approxi-

TABLE 2 Experimental and calculated distributions of aggregate sizes

Vesicles per aggregate	Apparent distribution* Experimental§	Apparent distribution* Calculated	Apparent distribution* Calculated‖ (30% bivalent)	Corrected distribution*‡ Experimental	Corrected distribution*‡ Calculated	Corrected distribution*‡ Calculated‖ (30% bivalent)
At t = 2 min						
1	58 ± 2	55	56	41 ± 2	34	36
2	21 ± 1	25	25	26 ± 2	23	24
3	11 ± 1	13	12	8 ± 3	20	19
≥4	10 ± 1	7	7	26 ± 2	23	21
At t = 6 min						
1	44 ± 2	41	44	27 ± 3	28	32
2	22 ± 2	19	21	15 ± 3	17	20
3	20 ± 2	17	16	32 ± 4	17	17
≥4	14 ± 2	23	19	26 ± 4	38	31
At t = 15 min						
1	39 ± 3	37	40	21 ± 3	28	32
2	15 ± 3	15	17	6 ± 4	16	19
3	17 ± 3	14	14	25 ± 5	15	16
≥4	29 ± 3	34	29	47 ± 7	41	33
Best fit C (M^{-1} s^{-1})		3×10^4	3×10^4		8×10^4	9×10^4
Best fit D (s^{-1})		0.006	0.006		0.008	0.008
RMS error in fit¶		4.2	2.9		9.3	10.2

* Percent of vesicles in each aggregate size.
‡ Based on stereological correction.
§ Range is standard deviation based on Poisson counting statistics for the vesicles.
‖ Assuming 30% of the MAb binds bivalently intravesicularly and is removed from the aggregation process.
¶ Computed as $[\Sigma\ (\text{calc}_i\text{-exptl}_i)^2/(N-2)]^{1/2}$, where i runs over the N = 12 data points (four aggregate sizes times three time points).

TABLE 3 **Calculated effect of MAb/vesicle ratio on aggregation process***

	MAb per vesicle‡		
Vesicles per aggregate	1.1	2.3	4.5
At t = 1 min			
1	82	74	65
2	15	19	23
3	2	5	9
≥4	1	2	3
At t = 2 min			
1	75	63	54
2	19	22	22
3	5	10	14
≥4	1	5	10
At t = 6 min			
1	67	48	32
2	19	16	10
3	8	13	14
≥4	6	23	44

* The kinetic parameters are those obtained for the corrected distribution: $C = 9 \times 10^4\ M^{-1}\ s^{-1}$ and $D = 0.008\ s^{-1}$, assuming 30% intravesicular binding of the MAb. Vesicle concentration is 0.1 μM, and the percents of vesicles without available antibodies for intervesicular bivalent binding are 50, 24, and 4, for 1.1, 2.3, and 4.5 MAb/vesicle, respectively.

‡ Distribution (percent of vesicles in each aggregate size).

mate model. Nevertheless, it is noteworthy that attaching the reactants to vesicles has much smaller effects on affinity than on kinetics.

We have used the model to predict the effects of MAb/vesicle ratio on the aggregation process. Table 3 shows the results for 1.1, 2.3, and 4.5 MAb per vesicle under conditions identical to those for the turbidimetric experiments reported in Fig. 4 *B*. Although the actual distribution of aggregates cannot be deduced from turbidity measurements and it is hard to calculate changes in turbidity from the known distribution of aggregates, we can make qualitative comparisons between the theoretical and turbidimetric results. We may take the percent of vesicles in monomers or the average aggregate size as a measure for the development of the aggregation process. A comparison of Table 2 with Table 3 (first column, 1.1 MAb per vesicle) indicates that for the same time points, e.g., 2 and 6 min, there is less aggregation in the latter case because of fourfold reduction in vesicle concentration. According to Table 3, the aggregation process is more developed for the case with 2.3 MAb per vesicle at 1 and 2 min than for the case with 1.1 MAb per vesicle at 2 and 6 min, respectively. This is in accord with the turbidity results in Fig. 4 *B*. A similar agreement holds for additional cases, but overall the turbidity data depend more steeply on MAb/vesicle ratio than do the theoretical results in Table 3. This partly may be due to nonlinearities in the relationship between turbidity and extent of aggregation. It probably also results from the way the theory incorporates the MAb/vesicle ratio: adding more MAbs decreases the number of vesicles without antibodies but it does not formally increase C or decrease D as the number of antibodies bound per vesicle increases. Hence, the theory is most applicable at low MAb/vesicle ratios. In addition, we can anticipate that more intravesicular binding should occur at lower concentrations of vesicles used for Fig. 4 *B* and that the probability of intravesicular binding should decrease in the presence of larger ratios of MAb/vesicle. We have not explicitly accounted for these effects since the simulation of the EM results focussed on the 1.1 ratio and more concentrated vesicle suspensions.

CONCLUSION

The antibody-hapten mediated aggregation of vesicles is a convenient model for more complex biological systems, such as virus–cell or cell–cell interactions, since we had the advantage of varying both receptor (hapten) and ligand (antibody) concentrations. We have shown that at low (micromolar) lipid concentrations the system displays relatively classical precipitin behavior with some MAbs. Others produce scant precipitation. We suggest that antibody affinity is an important determinant of this behavior: sufficiently high-affinity antibodies bind bivalently to a single vesicle and are kinetically unable to participate in aggregation. At high (millimolar) lipid concentrations, we have followed the aggregation by EM and turbidimetry and by a theoretical model based on mass-action kinetics. We have reported the morphologies of small aggregates and have found that the rates of the process are slowed by orders of magnitude compared either with the binding of antibodies to hapten-containing vesicles or with the cation-induced aggregation of negatively charged vesicles. The apparent affinity for aggregating vesicles is reduced less.

We thank D. Friend, UC San Francisco, for his advice and help on freeze-fracture EM. The EM work was enormously facilitated by the staff of the EM Laboratory at the University of California, Berkeley, especially by C. Schooley. Hybridomas were generously given by E. W. Voss, Jr.

This work was supported by National Institutes of Health grant AI-22860 (J. C. Owicki), and by grant AI-25534 (N. Düzgünes and S. Nir) and partially by Schonbrunn Funds from the Hebrew University of Jerusalem (S. Nir).

Received for publication 29 April 1992 and in final form 1 November 1992.

REFERENCES

Bearer, E. L., N. Düzgünes, D. S. Friend, and D. Papahadjopoulos. 1983. Fusion of phospholipid vesicles arrested by quick freezing. The question of lipidic particles as intermediates in membrane fusion. *Biochim. Biophys. Acta.* 693:93–98.

Bentz, J., and S. Nir. 1981. Mass action kinetics and equilibria of reversible aggregation. *J. Chem. Soc. Faraday Tran. I.* 77:1249–1275.

Bentz, J., S. Nir, and D. G. Covell. 1988. Mass action kinetics of virus-cell aggregation and fusion. *Biophys. J.* 54:449–462.

Berg, H. C., and E. M. Purcell. 1977. Physics of chemoreception. *Biophys. J.* 20:193–220.

Bongrand, P., and G. I. Bell. 1984. Cell-cell adhesion: parameters and possible mechanisms. *In* Cell Surface Dynamics: Concepts and Models. A. S. Perelson, C. DeLisi, and F. W. Wiegel, editors. Marcel Dekker, Inc., New York and Basel. 459–493.

Crothers, D. M., and H. Metzger. 1972. The influence of polyvalency on the binding properties of antibodies. *Immunochemistry.* 9:341–357.

Curatolo, W., A. O. Yau, D. M. Small, and B. Sears. 1978. Lectin-induced agglutination of phospholipid/glycolipid vesicles. *Biochemistry.* 17:5740–5746.

Day, E. P., A. Y. Kwok, S. K. Hark, J. T. Ho, W. J. Vail, J. Bentz, and S. Nir. 1980. Reversibility of sodium-induced aggregation of sonicated phosphatidylserine vesicles. *Proc. Natl. Acad. Sci. USA.* 77:4026–4029.

DeLisi, C. 1974. A theory of precipitation and agglutination reactions in immunological systems. *J. Theor. Biol.* 45:555–575.

DeLisi, C. 1980. The biophysics of ligand-receptor interactions. *Q. Rev. Biophys.* 13:201–230.

Edelman, G. M. 1983. Cell adhesion molecules. *Science (Wash. DC).* 219:450–457.

Gilkey, J., and L. A. Staehelin. 1986. Advances in ultra-rapid freezing for preservation of cellular ultrastructure. *J. Electron Microsc. Tech.* 3:177–210.

Goodwin, G. C., K. Hammond, I. G. Lyle, and M. N. Jones. 1982. Lectin-mediated agglutination of liposomes containing glycophorin. *Biochim. Biophys. Acta.* 689:80–88.

Heidelberger, M., and F. E. Kendall. 1935. A quantitative theory of the precipitin reaction. III. The reaction between crystalline egg albumin and its homologous antibody. *J. Exp. Med.* 62:697–720.

Heuser, J. E., and T. S. Reese. 1981. Structural changes after transmitter release at the frog neuromuscular junction. *J. Cell Biol.* 88:564–580.

Hoekstra, D., and J. W. Kok. 1989. Entry mechanisms of enveloped viruses. Implications for fusion of intracellular membranes. *Biosci. Rep.* 9:273–305.

Hui, S. W., S. Nir, T. P. Stewart, L. T. Boni, and S. K. Huang. 1988. Kinetic measurements of fusion of phosphatidylserine-containing vesicles by electron microscopy and fluorometry. *Biochim. Biophys. Acta.* 941:130–140.

Kachar, B., N. Fuller, and R. P. Rand. 1986. Morphological responses to calcium-induced interaction of phosphatidylserine-containing vesicles. *Biophys. J.* 50:779–788.

Kantor, A. B. 1988. Monoclonal antibody interactions with hapten-bearing liposomes. Ph.D. dissertation. University of California, Berkeley. 170 pp.

Kantor, A. B., S. G. Stanton, and J. C. Owicki. 1986. Aggregation of hapten-bearing liposomes by antibody. *Biophys. J.* 49:118*a*. (Abstr.)

Klinman, N. R., and F. Karush. 1967. Equine anti-hapten antibody. V. The non-precipitability of bivalent antibody. *Immunochemistry.* 4:387–405.

Kranz, D. M., and E. W. Voss, Jr. 1981. Partial elucidation of an anti-hapten repertoire in BALB/c mice: comparative characterization of several monoclonal anti-fluorescyl antibodies. *Mol. Immunol.* 18:889–898.

Kung, V. T., P. E. Maxim, R. W. Veltri, and F. J. Martin. 1985. Antibody-bearing liposomes improve agglutination of latex particles used in clinical diagnostic assays. *Biochim. Biophys. Acta.* 839:105–109.

Lee, K.-D. 1988. Ligand-receptor mediated membrane-membrane interactions: An electron microscopy study of a model system, Ph.D. Dissertation, University of California, Berkeley. 132 pp.

Lee, K.-D., and J. C. Owicki. 1989*a*. Aggregation of hapten-bearing liposomes by antibodies: an electron microscopy study of kinetics and aggregate morphology. *Biophys. J.* 55:323*a*. (Abstr.)

Lee, K.-D., and J. C. Owicki. 1989*b*. A rapid freezing and freeze-fracturing method applied to the aggregation of hapten-bearing liposomes. *J. Electron Microsc. Tech.* 13:372–373.

Luedtke, R., and F. Karush. 1982. Antibody interaction with a membrane-bound fluorescent ligand on synthetic lipid vesicles. *Biochemistry.* 21:5738–5744.

Mansbach, L., M. Becker, M. Gallagher, and S. Pearlman. 1985. Development of a liposome based fluorescent immunoassay for serum digoxin. *Clin. Chem.* 31:830.

Mason, D. W., and A. F. Williams. 1980. The kinetics of antibody binding to membrane antigens in solution and at the cell surface. *Biochem. J.* 187:1–20.

Mayer, L. D., M. J. Hope, and P. R. Cullis. 1986. Vesicles of variable sizes produced by a rapid extrusion procedure. *Biochim. Biophys. Acta.* 858:161–168.

Moller, N. P. H. 1979. Fc-mediated immune precipitation. I. A new role of the Fc-portion of IgG. *Immunology.* 38:641–648.

Nelsestuen, G. L., and T. K. Lim. 1977. Equilibria involved in prothrombin- and blood-clotting factor X-membrane binding. *Biochemistry.* 16:4164–4177.

Nir, S., J. Bentz, J. Wilschut, and N. Düzgünes. 1983. Aggregation and fusion of phospholipid vesicles. *Prog. Surf. Sci.* 13:1–124.

Nir, S., T. Stegmann, and J. Wilschut. 1986*a*. Fusion of influenza virus with cardiolipin liposomes at low pH: mass action analysis of kinetics and fusion. *Biochemistry.* 25:257–266.

Nir, S., K. Klappe, and D. Hoekstra. 1986*b*. Kinetics and extent of fusion between Sendai virus and erythrocyte ghosts: application of a mass action kinetic model. *Biochemistry.* 25:2155–2161.

Nir, S., N. Düzgünes, M. C. Pedroso de Lima, and D. Hoekstra. 1990. Fusion of enveloped viruses with cells and liposomes: activation and inactivation. *Cell Biophys.* 17:181–201.

Ohnishi, S.-I. 1988. Fusion of viral envelopes with cellular membranes. *In* Membrane Fusion in Fertilization, Cellular Transport and Viral Infection. N. Düzgünes and F. Bronner, editors. Academic Press, San Diego. 257–296.

Oi, V. T., T. M. Vuong, R. Hardy, J. Reidler, J. Dangl, L. A. Herzenberg, and L. Stryer. 1984. Correlation between segmental flexibility and effector function of antibodies. *Nature (Lond.).* 307:136–140.

Petrossian, A., and J. C. Owicki. 1984. Interactions of antibodies with fluorescent haptenated phospholipid vesicles. *Biochim. Biophys. Acta.* 776:217–227.

Petrossian, A., A. B. Kantor, and J. C. Owicki. 1985. Synthesis and characterization of a highly fluorescent peptidylphosphatidylethanolamine. *J. Lipid Res.* 26:767–773.

Reinitz, D. M., and E. W. Voss, Jr. 1984. Idiotypic cross-reactivity of low-affinity antifluorescyl monoclonal antibodies. *Mol. Immunol.* 21:775–784.

Smoluchowski, M. 1917. Investigation into the mathematical theory of the kinetics of coagulation of colloidal solutions. *Z. Phys. Chem. Abteil A.* 92:129–168.

Springer, T. A. 1990. Adhesion receptors of the immune system. *Nature (Lond.).* 346:425–434.

Stanton, S. G., A. B. Kantor, A. Petrossian, and J. C. Owicki. 1984. Location and dynamics of a membrane-bound fluorescent hapten: a spectroscopic study. *Biochim. Biophys. Acta.* 776:228–236.

Szoka, F., F. Olson, T. Heath, W. Vail, E. Mayhew, and D. Papahadjopoulos. 1980. Preparation of unilamellar liposomes of intermediate size (0.1–0.2 μm) by a combination of reverse phase evaporation and extrusion through polycarbonate membranes. *Biochim. Biophys. Acta.* 601:559–571.

von Schulthess, G. K., R. J. Cohen, N. Sakato, and G. Benedek. 1976. Laser light scattering spectroscopic immunoassay for mouse IgA. *Immunochemistry.* 13:955–962.